

# The 2011 Periastron Passage of the Be Binary $\delta$ Scorpii

A. S. Miroshnichenko<sup>1</sup>

<sup>1</sup>*Department of Physics and Astronomy, University of North Carolina at Greensboro,  
Greensboro, NC 27402-6170, USA*

A. V. Pasechnik<sup>2</sup>

<sup>2</sup>*Tuorla Observatory, Department of Physics and Astronomy, University of Turku, Finland*

N. Manset<sup>3</sup>

<sup>3</sup>*CFHT Corporation, 65-1238 Mamalahoa Hwy, Kamuela, HI 96743*

A. C. Carciofi<sup>4</sup>

<sup>4</sup>*Instituto de Astronomia, Geofísica e Ciências Atmosféricas, Universidade de São Paulo,  
Brazil*

Th. Rivinius<sup>5</sup>

<sup>5</sup>*European Southern Observatory, Chile*

S. Štefl<sup>5,6</sup>

<sup>5</sup>*European Southern Observatory, Chile*

<sup>6</sup>*Joint ALMA Observatory, Chile*

V. V. Gvaramadze<sup>7,8</sup>

<sup>7</sup>*Sternberg Astronomical Institute, Lomonosov Moscow State University, Universitetskij Pr.  
13, Moscow 119992, Russia*

<sup>8</sup>*Isaac Newton Institute of Chile, Moscow Branch, Universitetskij Pr. 13, Moscow 119992,  
Russia*

J. Ribeiro<sup>9</sup>

<sup>9</sup>*Observatorio do Instituto Geografico do Exercito, Lisboa, Portugal*

A. Fernando<sup>10</sup>

<sup>10</sup>*ATALAIA.org Group—Lisboa, Portugal*

T. Garrel<sup>11</sup>

<sup>11</sup>*Observatoire de Foncaude, Montpellier, France*

J. H. Knapen<sup>12,13</sup>

<sup>12</sup>*Instituto de Astrofísica de Canarias, E-38205 La Laguna, Tenerife, Spain*

<sup>13</sup>*Departamento de Astrofísica, Universidad de La Laguna, 38206 La Laguna, Spain*

C. Buil<sup>14</sup>

<sup>14</sup>*Castanet Tolosan Observatory, Toulouse, France*

B. Heathcote<sup>15</sup>

<sup>15</sup>*Barfold Observatory, Glenhope, Victoria 3444, Australia*

E. Pollmann<sup>16</sup>

<sup>16</sup>*Emil-Nolde-Str. 12, 51375, Leverkusen, Germany*

B. Mauclaire<sup>17</sup>

<sup>17</sup>*Observatoire du Val d'Arc, France*

O. Thizy<sup>18</sup>

<sup>18</sup>*Shelyak Instruments, France*

J. Martin<sup>19</sup>

<sup>19</sup>*Barber Research Observatory, Department of Physics and Astronomy, University of Illinois-Springfield, IL 62703, USA*

S. V. Zharikov<sup>20</sup>

<sup>20</sup>*Instituto de Astronomía, Universidad Nacional Autónoma de México, Apdo. Postal 877, Ensenada, 22800, Baja California, México*

A. T. Okazaki<sup>21</sup>

<sup>21</sup>*Faculty of Engineering, Hokkai-Gakuen University, Toyohira-ku, Sapporo 062-8605, Japan*

T. L. Gandet<sup>22</sup>

<sup>22</sup>*Lizard Hollow Observatory, P.O. Box 89175, Tucson, AZ 85752-9175, USA*

T. Eversberg<sup>23</sup>

<sup>23</sup>*Schnörringen Telescope Science Institute, Waldbröl, Germany*

N. Reinecke<sup>24</sup>

<sup>24</sup>*Bonn, Germany*

## ABSTRACT

We describe the results of the world-wide observing campaign of the highly eccentric Be binary system  $\delta$  Scorpii 2011 periastron passage which involved professional and amateur astronomers. Our spectroscopic observations provided a precise measurement of the system orbital period at  $10.8092 \pm 0.0005$  years. Fitting of the He II 4686 Å line radial velocity curve determined the periastron passage time on 2011 July 3, UT 9:20 with a 0.9-day uncertainty. Both these results are in a very good agreement with recent findings from interferometry. We also derived new evolutionary masses of the binary components (13 and 8.2  $M_{\odot}$ ) and a new distance of 136 pc from the Sun, consistent with the HIPPARCOS parallax. The radial velocity and profile variations observed in the H $\alpha$  line near the 2011 periastron reflected the interaction of the secondary component and the circumstellar disk around the primary component. Using these data, we estimated a disk radius of 150  $R_{\odot}$ . Our analysis of the radial velocity variations measured during the periastron passage time in 2000 and 2011 along with those measured during the 20th century, the high eccentricity of the system, and the presence of a bow shock-like structure around it suggest that  $\delta$  Sco might be a runaway triple system. The third component should be external to the known binary and move on an elliptical orbit that is tilted by at least 40° with respect to the binary orbital plane for such a system to be stable and responsible for the observed long-term radial velocity variations.

---

<sup>1</sup>This paper is partially based on observations obtained at the Canada-France-Hawaii Telescope (CFHT) which is operated by the National Research Council of Canada, the Institut National des Sciences de l'Univers of the Centre National de la Recherche Scientifique de France, and the University of Hawaii, the 2.2m MPG telescope operated at ESO/La Silla under program IDs 086.A-9019 and 087.A-9005, the IAC80 telescope in the Spanish Observatorio del Teide of the Instituto de Astrofísica de Canarias, and data from the ELODIE archive at the Observatoire de Haute-Provence.

*Subject headings:* Stars: emission-line, Be; (Stars:) binaries: spectroscopic; Stars: individual:  $\delta$  Sco

## 1. Introduction

$\delta$  Scorpii is one of the brightest stars in the sky. Until 2000, its visual brightness was  $V = 2.32$  mag; since then, and due to its transition to a Be phase (Carciofi et al. 2006), it has been even brighter ( $V \leq 1.6$  mag). It was resolved interferometrically into two components in the 1970's, and the observations indicated a very eccentric orbit with a period of  $\sim 10.6$  years (Hartkopf et al. 1996). The system is not eclipsing, and the secondary component is  $\Delta B = 1.78 \pm 0.03$  mag fainter than the primary one (Tango et al. 2009).

$\delta$  Sco was used as a spectral classification standard (B0 IV) during the entire 20th century. The first signs of weak emission in the  $H\alpha$  line were detected by Côté & van Kerkwijk (1993) close to a periastron time in 1990, but the emission only slightly varied throughout the next orbital cycle (Miroshnichenko et al. 2001; Koubský 2005). In June 2000, near the following periastron time, the system was found to be  $\sim 0.03$  mag brighter than usual, while a spectrum taken shortly after revealed a noticeable  $H\alpha$  emission line (Fabregat, Reig, & Otero 2000). A follow up spectroscopic campaign resulted in the detection of a growing line emission and a significant variation of the radial velocity (Miroshnichenko et al. 2001). These data constrained the periastron time (2000 September  $9 \pm 3$ ) which was predicted to occur a few months earlier from the interferometric data. Since that time the circumstellar (CS) disk around the primary component of  $\delta$  Sco grew larger, the system brightness varied between  $V \sim 1.6$  and 2.3 mag, but the line emission has never disappeared. The disk development has been documented in Miroshnichenko et al. (2003) and Carciofi et al. (2006).

The erroneous interferometric prediction of the periastron time in 2000 reflected the accuracy of this technique at that time. The orbital separation of the components that varies from 6 to 200 mas only allowed to resolve them during about half the orbital cycle, mostly around apastron. Recent advances in this field made it possible to cover the entire orbit (e.g., Tycner et al. 2011; Meilland et al. 2011). The interferometric observations obtained since 2000 combined with the orbit derived from the radial velocity curve (Miroshnichenko et al. 2001) resulted in predicting the periastron time in 2011 with a high accuracy (2011 July 2–6, Tango et al. 2009; Tycner et al. 2011; Meilland et al. 2011). Moreover, interferometry obtained in July 2011 (Che et al. 2012; Štefl et al. 2012), right after the periastron, confirmed the prediction.

Spectroscopy is another powerful tool in studying binaries that is capable of verifying interferometric results and obtaining additional information about objects’ properties. In order to get ready for the 2011 periastron, a spectroscopic observing campaign was planned well in advance (e.g., Miroshnichenko 2009). Its important feature was a broad participation of amateur astronomers whose involvement in spectroscopic observations of various objects significantly increased over the last decade (e.g., Fahed et al. 2011).

This paper describes the main results of the  $\delta$  Sco 2011 periastron spectroscopic observing campaign as well as some additional findings that suggest new ideas about the system’s nature and evolution. The observations are described in Sect. 2, analysis of the 2011 periastron radial velocity curves and the orbital period determination are presented in Sect. 3, historical radial velocity data along with new ideas about the system’s nature are discussed in Sect. 4, and conclusions and predictions are summarized in Sect. 5.

## 2. Observations

Spectroscopic monitoring of  $\delta$  Sco began shortly after its brightening discovery in 2000 (Fabregat, Reig, & Otero 2000) and has been ongoing since that time. Due to its brightness, it has mostly been observed with under 1m size telescopes. The amateur community participation has been steadily growing towards the time of the 2011 periastron. While only a few spectra of  $\delta$  Sco were obtained by amateurs in 2000, this number grew to 200 spectra in 83 nights in 2010 and over 300 spectra in 149 nights in 2011. The amateurs contribution in 2010–2011 is comparable with that of professional astronomers in the number of spectra and exceeds it in the time coverage.

The main goals of the 2011 campaign were 1) to obtain an accurate radial velocity curve to independently constrain the orbital period, and 2) to study line profile variations to search for effects of the interaction between the disk and the secondary component as well as possibly get information about the latter. The interaction was expected due to a very small distance between the components at periastron ( $\sim 15$  radii of the primary component, Miroshnichenko et al. 2001) and the disk size comparable with this distance (Carciofi et al. 2006; Millan-Gabet et al. 2010).

Since not all of the involved observers were able to cover a wide spectral range, it was suggested to focus on the two following regions. First, a region around the  $H\alpha$  emission line whose profile is indicative of the tidal interaction due to a possible disk restructuring. Second, a region around the photospheric He II 4686 Å line whose profile seems to be the least affected by the disk material and is therefore the best tracer of the orbital motion of

the primary component. The He I lines that are abundant in the object’s spectrum were rejected because their profiles are subject to complicated distortions by the disk material, and the CS contribution to them is difficult to quantify.

The main instruments that contributed to the campaign from the professional side were the 3.6 m CFHT with the spectropolarimeter ESPaDOnS (Donati et al. 1997), which covers a region  $\sim 3600\text{--}10\,500\text{ \AA}$  with a spectral resolving power  $R \sim 70\,000$ , and the 2.2 m MPG telescope at ESO/La Silla with the FEROS spectrograph (Kaufer et al. 2000), which covers a region  $\sim 3600\text{--}9200\text{ \AA}$  with  $R = 48\,000$ . Over 300 individual spectra of  $\delta$  Sco were obtained at these facilities during 40 nights in 2011.

An important feature of the campaign was a ten night observing run at the 0.8 m IAC80 telescope of the Instituto de Astrofísica de Canarias at the Teide Observatory on the Canary Island of Tenerife in Spain. The run took place between 2011 June 28 and 2011 July 8, was centered on the periastron time predicted by Tycner et al. (2011), and accomplished by a team of five authors of this paper (A. Miroschnichenko, J. Ribeiro, A. Fernando, T. Garrel, and J. Knapen). We used a private Lhires III spectrograph<sup>1</sup> with  $R \sim 17\,000$  in the H $\alpha$  region and  $R \sim 21\,000$  in the He II 4686  $\text{\AA}$  line region. All nights of the run were clear. We obtained over 100 individual exposures in the two mentioned regions as well as in a region near H $\gamma$  and He I 4471  $\text{\AA}$  line.

The amateur community contribution to the campaign involved nearly 20 observers from France, Germany, Australia, Portugal, Spain, and the USA. They used 0.2 m to 0.4 m telescopes with either échelle or long-slit spectrographs with a range of  $R = 1000\text{--}22\,000$ . Only the spectra with  $R \geq 10\,000$  were used in our analysis.

Data reduction was performed using Libre-ESpRIT data reduction package (Donati et al. 1997) for the ESPaDOnS data and ESO–MIDAS package for the FEROS data. IRAF was used to reduce some of the Tenerife campaign data, while most amateurs data were reduced with software packages developed for amateur spectrographs, such as Audela<sup>2</sup> and IRIS<sup>3</sup>. Wavelength calibration was controlled by measuring positions of telluric and interstellar (e.g., Na I D<sub>1,2</sub>) lines and contemporaneous observations of radial velocity standards (e.g.,  $\alpha$  Ser and  $\delta$  Oph). Typical uncertainties of the radial velocity measurements are below  $1\text{ km s}^{-1}$  for the ESPaDOnS and FEROS data and  $2\text{--}4\text{ km s}^{-1}$  for the amateur data.

---

<sup>1</sup><http://www.astrosurf.com/thizy/lhires3/index-en.html>

<sup>2</sup><http://www.audela.org/dokuwiki/doku.php/en/start>

<sup>3</sup>[http://www.astrosurf.com/buil/isis/isis\\_en.htm](http://www.astrosurf.com/buil/isis/isis_en.htm)

### 3. Data Analysis

#### 3.1. The H $\alpha$ line

The double-peaked structure of the H $\alpha$  line profile was resolved almost all the time in 2011 even at  $R \sim 10\,000$ . The peak intensity ratio was  $V/R \geq 1$  until about a month before the periastron time, then it reached a minimum at periastron, and came back to the pre-periastron value about two weeks later (see Fig. 1ab). The line equivalent width increased from  $\sim 11$  Å in May 2011 to  $\sim 15$  Å in September, while the visual continuum got brighter by  $\sim 0.1$  mag between late-June and a few days after the periastron (Rivinius et al. 2012). Therefore the line flux was rising as well. The latter is unlikely to be due to a tidally induced enhanced mass loss from the primary, as the close passage of the secondary only reduced the primary surface gravity by  $\sim 0.01\%$ . Both the  $V/R$  and the equivalent width changes began virtually at the same time and might be explained by emission from the disk material that was getting into the secondary Roche lobe. The secondary was moving away from us until the periastron time and might have caused the red peak enhancement.

The system brightness decreased after the periastron, and the above mentioned further increase of the equivalent width was mostly due to this effect. This is consistent with a constant disk contribution to the  $H$ -band flux from 6 to 18 days after periastron reported by Che et al. (2012). We also note that in 2010 the H $\alpha$  radial velocity was the same as before the 2000 periastron, but became  $\sim 10$  km s $^{-1}$  more negative in January 2011, nearly two months earlier than the radial velocity should have started to change due to the binary components closeness. This effect might have been due to some processes in the disk which are beyond the scope of this paper. A more detailed analysis of the line profile variations will be presented elsewhere (Rivinius et al., in prep.).

The radial velocity curve from the H $\alpha$  data is shown in Fig. 1cd. The measurements were accomplished using the mirrored profile method (see, e.g., Nemravová et al. 2012). The measurement results are presented in Table 1. The curve shows a more complicated structure compared to the one observed in 2000 and expected from a binary system with no changes in the CS matter. There were three turnovers marked by arrows in Fig. 1d. The first one occurred about five days before the periastron and was a consequence of the line profile redshift ( $V/R$  decrease) described above. The second one occurred two days after the periastron, when the  $V/R$  ratio exhibited a minimum. The third one took place nearly two weeks after the periastron on 2011 July 18 (JD2455760) and coincided with the rapid change of the  $V/R$  ratio back to  $\sim 1.1$ . After that time, the secondary with a part of the circumprimary disk seemed to have moved beyond the disk boundary and stopped affecting the remaining part of the disk.

The line profile variations near the periastron allow us to roughly estimate the disk radius. The changes began to occur about 10 days prior to the periastron, when the stars were  $\sim 250 R_{\odot}$  apart. Assuming an equilibrium situation, at this time the first Lagrangian point between the two stars was laying  $\sim 150 R_{\odot}$  from the primary (Eggleton 1983). This distance can be regarded as an upper limit on the disk radius. It corresponds to 20 radii of the primary component assuming a distance of 136 pc (see Sect. 3.4). This is somewhat larger than the  $104 R_{\odot}$  for the semi-major FWHM of the primary  $H\alpha$  disk measured by Millan-Gabet et al. (2010) in July 2007 during a brightness minimum period when the system was as bright as before the disk began developing.

The system became  $\sim 60\%$  optically brighter between 2009 and 2011. This brightening was very similar to the initial one in 2000/2001, but this time the disk was already present. The most likely reason for the fading was clearing of the disk inner regions due to the mass loss weakening (Haubois et al. 2012). However, the disk outer regions must have survived, as the line emission was observed all the time. Therefore, the circumprimary disk was probably steadily growing during the entire orbital cycle. It is beyond the scope of this paper to discuss this process in detail. We only note that the disk size was  $\sim 49 R_{\odot}$  already in 2001 (Carciofi et al. 2006), not in 2005 as quoted by Meilland et al. (2011).

The radial velocity of the  $H\alpha$  line continued to change very close to the binary model prediction since the end of July 2011 (solid line in Fig. 1d). Overall, the effects of the secondary close passage and its interaction with the disk made the  $H\alpha$  radial velocity curve broader than in 2000. Also, the  $H\alpha$  heliocentric radial velocity curve was shifted by  $\sim 6 \text{ km s}^{-1}$  to the negative velocities compared to that in 2000 (Fig. 1c). The shift may be due to a different disk density distribution as well as to other possible reasons discussed in Sect. 4.

### 3.2. The He II 4686 Å line

A spectral region that contains the He II 4686 Å line is shown in Fig. 2a. The radial velocity of the He II line was measured by fitting it to a Gaussian that for symmetric lines gives very similar results to the mirrored profile method. The measurement results are presented in Table 2. We have 115 measurements of the He II line radial velocity between 2010 May 28 and 2012 October 12. Eighty seven of them (from 2011 May 18 and September 8) were used in the radial velocity curve fitting. These include forty measurements from the ESPaDOnS and FEROS spectra, four from IAC80, and forty three from the amateurs spectra. The He II line profile kept stable, but its weakness ( $\sim 0.95$  of the continuum at the minimum intensity) seemed to be the source of scatter seen in Fig. 2b. In order to minimize the scatter, we averaged the measurements within 2–3 day intervals and fitted the resulting



25 data points to a binary orbital motion model predictions.

The initial orbital parameters for the fitting were taken from recent interferometry papers (e.g., Meilland et al. 2011; Che et al. 2012). Most of them are very close to the ones obtained for the 2000 data by Miroshnichenko et al. (2001). Nevertheless, we carried out an exhaustive least square fitting allowing all the orbital parameters to vary. We also fitted both the 2000 H $\alpha$  and 2011 He II data sets together to check for consistency of the orbital period determination. Using data for these two lines in the same set is legitimate because the disk in 2000 was very small and hardly affected by the secondary component approach. Therefore, the H $\alpha$  line very closely traced the motion of the primary component at that time. The best fit parameters are shown in Table 3. They are a little different for the 2000 data set, because this time we used the radial velocity semi-amplitude as a fit parameter instead of the semi-major axis, the component’s mass ratio, and the orbital inclination angle. However, the updated orbital elements are within the uncertainties given in Miroshnichenko et al. (2001) and also consistent with the recent interferometric solutions. The 2000 periastron epoch was refined from September  $9\pm 3$  to September  $10.5\pm 1.0$ .

The best fits to both the 2011 radial velocity data and the combined 2000 and 2011 data set show that the periastron occurred on 2011 July 3, 9:20 UT, with a 0.9–day uncertainty. Thus, the interferometric result for the periastron epoch (Che et al. 2012) was confirmed spectroscopically with a shift of only  $\sim 2$  hours, well within the uncertainties of both measurements. Our fitting also constrained the orbital period at  $3948.0\pm 1.8$  days, very close to the latest interferometric solutions.

The parameter errors presented in Table 3 are larger than those of the interferometric solution by Che et al. (2012). The main reason for this result is that the time period during which the radial velocity changes significantly is much shorter (2–3 months) than the system half orbital period during which interferometry data were taken. Nevertheless, spectroscopy provides an independent constraint for the radial velocity semi-amplitude which allows to derive the components masses (see Sect. 3.4).

The radial velocity curve derived for the He II line slightly deviates from the one derived for the H $\alpha$  line in 2000 (Fig. 2bc). It is slightly narrower and is shifted to the positive velocities by  $\sim 1.9\text{ km s}^{-1}$ . Although the deviation seems small, it may indicate that the orbit is unstable. We study this and other related observational features in Sect. 4.

### 3.3. Other Spectral Variations

There was a hope to detect signs of the secondary component in the spectrum due to a relatively large radial velocity difference at periastron ( $\sim 120 \text{ km s}^{-1}$ ). Some ideas about the secondary parameters were deduced from the system’s spectral energy distribution, orbital elements, and the components brightness ratio (an early B-type dwarf, see discussion in Miroshnichenko et al. 2001; Miroshnichenko 2009). One of the expected signatures of the secondary is shown in the left panel of Fig. 3. This prediction is based on a sum of two spectra taken from the online archive of the Observatoire de Haute Provence (OHP) obtained with the spectrograph ELODIE<sup>4</sup> ( $R \sim 48,000$ , Moulta et al. 2004). We chose the B0.5 v star BS 1880 to represent the primary and the B3 v star BS 801 to represent the secondary. The sum was calculated assuming a brightness ratio of  $\Delta B = 1.78 \text{ mag}$  (see Sect. 1). No CS continuum contribution was added to the composite spectrum, because we only aimed at a qualitative demonstration of possible effects at periastron.

Their projected rotational velocities listed in a recent catalog by Glebocki & Gnacinski (2005) are  $25\text{--}120 \text{ km s}^{-1}$  for BS 1880 and  $90\text{--}130 \text{ km s}^{-1}$  for BS 801. Although they are not as rapid rotators as  $\delta \text{ Sco}$  ( $v \sin i = 148\text{--}180 \text{ km s}^{-1}$  in the same catalog), we used these stars because their OHP spectra are clean and contain no other photospheric lines in the region between 4450 and 4500 Å except for the He I 4471 Å and Mg II 4482 Å. Intensity ratio of these two lines is one of the main temperature criteria for B-type stars. The Mg II line strengthens and the He I line weakens as the photospheric temperature decreases.

The composite spectrum may not be an accurate representation of the real situation due to uncertainties of the secondary component properties, but a broadening of the He I 4471 Å line profile was detected on the periastron day (Fig. 3b). This result can be interpreted as a detection of the secondary, although its parameters cannot be further constrained. However, it does not contradict the current view of this component (see also Meilland et al. 2011; Che et al. 2012).

### 3.4. The binary components masses and the system distance

There are several estimates for the mass of the primary component of  $\delta \text{ Sco}$  ( $M_1$ ) based on recent models of stellar evolution for the solar metallicity (e.g., Ekström et al. 2012) with ( $13.9 M_\odot$ , Che et al. 2012) or without ( $14.6 M_\odot$ , Pecaute, Mamajek, & Bubar 2012) taking into account gravity darkening due to the fast rotation of the star. Combining the

---

<sup>4</sup><http://atlas.obs-hp.fr/elodie/>

spectroscopic orbital solution derived here with the interferometry results (Che et al. 2012), one can estimate the components masses separately and derive the distance toward the system.

In order to do this, we calculate the system mass function ( $0.244 \pm 0.025 M_{\odot}$ ) from the data presented in Table 3. We also take into account the contribution of the secondary to the observed flux (see Sect. 1), which was mentioned but not considered by Pecaut, Mamajek, & Bubar (2012). This reduces the luminosity of the primary by 0.08 dex and its mass by  $0.2 M_{\odot}$  to  $M_1 = 14.4 M_{\odot}$  in the non-rotating case.

The components mass ratio ( $q_{1,2}$ ) depends on the orbital inclination angle ( $i$ ) and the mass function. It requires  $i = 36^{\circ} \pm 1^{\circ}$  to be consistent with the brightness ratio and comes to  $q_{1,2} = 1.67 \pm 0.07$ , giving an estimate for the secondary mass of  $M_2 = 8.6 \pm 0.6 M_{\odot}$ . The total mass of the binary implies an orbital semi-major axis of  $13.8 \pm 0.2$  AU. The latter combined with the angular measure of the semi-major axis from interferometry (99.04 mas, Che et al. 2012) gives a distance of  $140.0 \pm 1.5$  pc toward the system.

Rapid rotation creates a temperature distribution on a star’s surface that changes its fundamental parameters depending on the rotation rate and viewing angle (gravity darkening, Townsend, Owocki, & Howarth 2004). For  $\delta$  Sco that is viewed at an intermediate angle and rotates at  $\sim 60\%$  of the critical rate (estimated from  $v \sin i = 148 \text{ km s}^{-1}$ , Brown & Verschueren 1997), this effect increases its apparent luminosity by  $\sim 0.2$  dex and barely affects its apparent color. Taking this into account reduces  $M_1$  to  $13 M_{\odot}$  and for the same  $i = 36^{\circ} \pm 1^{\circ}$  changes  $q_{1,2}$  to  $1.6 \pm 0.1$ ,  $M_2$  to  $8.2 \pm 0.6 M_{\odot}$ , the orbital semi-major axis to  $13.5 \pm 0.1$  AU, and the distance to  $136.0 \pm 1.5$  pc.

Our estimates for  $M_2$  are consistent with its adopted spectral type (B1–B3,  $T_{\text{eff}} = 20000\text{--}24000$  K), while the distance toward the system is consistent with the HIPPARCOS parallax values from both published solutions ( $123_{-12}^{+15}$  and  $151_{-18}^{+23}$  pc, ESA 1997; van Leeuwen 2007, respectively). The new distance estimates are accounted for in the components luminosity calculation. This procedure resulted in a slightly larger orbital inclination angle compared to those determined from interferometry ( $30.2 \pm 0.7$ ,  $32.9 \pm 0.2$ ,  $32.3 \pm 0.3$ , Meilland et al. 2011; Tycner et al. 2011; Che et al. 2012, respectively). If  $i \leq 33^{\circ}$ , then  $M_2 \geq 10 M_{\odot}$  that is inconsistent with the reported components brightness ratio. No gravity darkening correction was applied to the secondary fundamental parameters, because no information about its rotation is currently available.

Also, the above fundamental parameters imply an age of 9–10 Myrs for both rotating and non-rotating primary mass estimates (Fig. 4). The theoretical positions for both secondary component models ( $8.6 M_{\odot}$  and  $8.2 M_{\odot}$ ) with an age of 10 Myrs are within the uncertainties

of our adopted parameters. The discrepancy does not seem to be dramatic and may be due to the unknown mass transfer history for the  $\delta$  Sco system as well as not well constrained spectral properties of the secondary component.

Both sets of the mass estimates are close to each other, but the one with gravity darkening taken into account seems to be more realistic. This subject will be explored in more detail in a separate study of the system’s spectral energy distribution.

#### 4. A New View of the $\delta$ Sco System

There are several facts that make  $\delta$  Sco unusual among Be binaries. First, the Bright Star Catalog (Hoffleit & Jaschek 1991) mentions a possible companion with a 20 day orbital period in the system (initially reported by van Hoof, Bertiau, & Deurinck 1963). Second, most Be binaries with a non-degenerate secondary component have circular orbits (e.g., Bjorkman et al. 2002; Nemravová et al. 2012), while most Be/X-ray binaries have eccentric orbits (e.g., Reig, Fabregat, & Coe 1997). Third, radial velocities of  $\delta$  Sco reported in several papers throughout the 20th century show variations additional to those expected at periastra (see Sect. 4.2). The difference between the 2000 and 2011 radial velocity curves reported above may be part of the same issue. Finally, thanks to the *IRAS* survey of bow shocks around runaway stars (van Buren, Noriega-Crespo, & Dgani 1995),  $\delta$  Sco is known as a bow-shock-producing star.

Taken together, the above facts allow us to suggest the hypothesis that  $\delta$  Sco might be a runaway triple system (cf., Gvaramadze & Menten 2012). A number of Be stars are known to be part of triple and more complex stellar systems (e.g., Koubský et al. 2010). Below we discuss the above mentioned facts more closely and conclude whether our hypothesis is viable.

##### 4.1. Possible origin of the high orbital eccentricity and the runaway status of the $\delta$ Sco system

The system orbital eccentricity is so large that component A (the Be star) and B (the interferometrically detected one) at periastron come together at a distance of  $\leq 0.8$  AU. There are several processes that can lead to such a highly eccentric orbit: a) close dynamical encounter between a binary system and another binary or a single star (e.g., Hills 1975; Hoffer 1983), b) dynamical decay of a trapezium-like system (Allen & Poveda 1974), and c) the Lidov-Kozai resonance in a hierarchical triple system (Lidov 1962; Kozai 1962).

The first process could also be responsible for ejection of  $\delta$  Sco from the parent star cluster (e.g., Leonard & Duncan 1990; Kroupa 1998). The ejection event might have occurred when the cluster was much smaller in size and much denser. This scenario is consistent with the presence of the bow shock-like structure around  $\delta$  Sco which is likely the result of the system (super)sonic motion through the interstellar medium.

To check the runaway status of  $\delta$  Sco, we used the proper motion measurements for this system from the new reduction of the *Hipparcos* data by van Leeuwen (2007),  $\mu_\alpha \cos \delta = -10.21 \pm 1.01$  mas yr<sup>-1</sup>,  $\mu_\delta = -35.41 \pm 0.71$  mas yr<sup>-1</sup> or, in Galactic coordinates,  $\mu_l = -32.22 \pm 0.87$  mas yr<sup>-1</sup> and  $\mu_b = -17.83 \pm 0.87$  mas yr<sup>-1</sup>. After correction for the Galactic differential rotation and the solar peculiar motion<sup>5</sup>, this proper motion translates into the transverse peculiar velocity  $v_{\text{tr}} = (v_l^2 + v_b^2)^{1/2} = 11.1 \pm 0.6$  km s<sup>-1</sup>, where  $v_l = -7.0 \pm 0.6$  km s<sup>-1</sup> and  $v_b = -8.6 \pm 0.6$  km s<sup>-1</sup>. To this velocity one should add a peculiar radial velocity of  $4.9 \pm 0.2$  km s<sup>-1</sup>, derived from the systemic radial velocity of  $-6.7 \pm 0.2$  km s<sup>-1</sup> (Meillard et al. 2011), so that the total (three-dimensional) velocity of  $\delta$  Sco  $v_* \approx 12$  km s<sup>-1</sup>, and its vector is inclined to the plane of the sky by an angle of  $\approx 34^\circ$ . Thus,  $\delta$  Sco is a low-velocity runaway system (cf. Gvaramadze et al. 2012). In their Figure 4, Peri et al. (2012) presented a  $22 \mu\text{m}$  image of an arc-like structure around  $\delta$  Sco taken by the *Wide-field Infrared Survey Explorer* (*WISE*, Wright et al. 2010). One can see that the vector of the peculiar transverse velocity of the star is almost parallel to the symmetry axis of the structure, which supports its interpretation as a bow shock.

$\delta$  Sco is located within the confines of the Sco OB2 association, and the distances to both systems are comparable to each other. This might imply that Sco OB2 is the parent association of  $\delta$  Sco. To check this possibility, one should compare the proper motion of  $\delta$  Sco with that of Sco OB2,  $\mu_l = -23.5 \pm 2.9$  mas yr<sup>-1</sup> and  $\mu_b = -10.5 \pm 4.0$  mas yr<sup>-1</sup> (Melnik & Dambis 2009), which also is based on the new reduction of the *Hipparcos* data by van Leeuwen (2007). This comparison shows that although both objects are moving almost in the same direction, there is a significant difference in the magnitudes of their proper motions. This difference could partially be caused by the effect of binarity of  $\delta$  Sco, because, as noted by de Zeeuw et al. (1999), “the *HIPPARCOS* proper motion, observed during the mission lifetime of  $\sim 3.3$  yr, does not necessarily reflect the center-of-mass proper motion”. This difference, however, could also be caused by the runaway status of  $\delta$  Sco. Moreover, one cannot exclude the possibility that the effect of binarity could instead be responsible for some *reduction* of the difference in the proper motions. Taken at face value, the observed proper motions imply that  $\delta$  Sco is moving with a transverse velocity of  $7.5$  km s<sup>-1</sup> with

---

<sup>5</sup>Here we used the Galactic constants  $R_0=8.0$  kpc and  $\Theta_0=240$  km s<sup>-1</sup> (Reid et al. 2009) and the solar peculiar motion  $(U_\odot, V_\odot, W_\odot) = (11.1, 12.2, 7.3)$  km s<sup>-1</sup> (Schonrich, Binney, & Dehnen 2010).

respect to the association. From this, in turn, it follows that the birth place of this  $\sim 10$  Myr old star should be at  $\approx 30^\circ$  from the birth place of the association (provided that the age of the association is  $\sim 10$  Myr as well). We conclude therefore that it is likely that  $\delta$  Sco was injected in the Sco OB2 association from outside (cf. Gvaramadze, Pflamm-Altenburg, & Kroupa 2011; Gvaramadze et al. 2012) and that the parent cluster of this star is located at  $\sim 50^\circ$  from its current position.

We also note that it has recently been found that the orbital momentum of the secondary and the disk’s rotation vector are opposite to each other (Štefl et al. 2012; Che et al. 2012). This might imply that the  $\delta$  Sco system was formed in the course of a few-body dynamical interaction or could be a consequence of the Lidov-Kozai resonance, if the system is triple. Detailed discussion of these possibilities, however, is beyond the scope of this paper.

#### 4.2. Stability of the binary orbital period

We will use radial velocity data published during the 20th century (Frost et al. 1926; van Hoof, Bertiau, & Deurinck 1963; Thackeray 1966; Beardsley 1969; Levato et al. 1987) to search for the binary orbital period variations. These papers present 49 measurements obtained between 1902 and 1976. The data along with those from Miroschnichenko et al. (2001) and this work are shown in Fig. 5. Most of the historical data deviate from the expected radial velocity behavior based on the modern solution. This can be partly due to both random and systematic errors. For example, Beardsley (1969) concluded that the Allegheny observatory data presented in his work showed no variations and can be averaged. Still, some data points from Frost et al. (1926) and Beardsley (1969) match with the expected radial velocity minima due to the periastron passages.

We investigated both the historical (20th century only) and full data sets using the methods for finding periodicity from Dworetzky (1983) and Scargle (1982). Both methods are suited for unevenly spaced data, but Scargle’s method works better for nearly sinusoidal variations. The historical data miss most of the radial velocity minima that result in not well-defined extrema of the periodograms. The Dworetzky “string-length” function shows the deepest minimum for a period of 3750 days for the historical data, while the Scargle periodogram shows the highest maximum for a period of 3339 days. In both cases, it is at least 200 days shorter than the one determined from the periastra of 2000 and 2011.

Nevertheless, both methods detected the modern period when fitting the entire data collection. Dworetzky’s function peaks at 3928 days, while Scargle’s one at 3915 days. The shifts toward shorter periods are due to the historical data. They can be caused by the

variable orbital period and/or errors in the radial velocity measurements.

Although the existing material does not allow us to make a definite conclusion about the reality of these shifts, it prompts us to analyze the role of a possible third component in the system in the origin of changes in the orbital period. We also examine the stability of triple systems and show that under the certain conditions the presence of the third component could be responsible for maintaining the system’s high eccentricity.

### 4.3. Analysis of the long-term radial velocity variations

Let us now consider stability of triple systems that may result in the observed radial velocity variations. Orbital solutions in general require numerical integration, but approximations can be obtained in some cases. In particular, stability conditions for hierarchical triple systems with a low eccentricity of the inner pair are given by the following formula (Valtonen et al. 2008):

$$\left(\frac{q}{a_i}\right) > 3 \left(1 + \frac{m_3}{m_1 + m_2}\right)^{1/3} (1 - e)^{-1/6} \left(\frac{1 + \cos \iota}{2}\right)^{1/3} \quad (1)$$

where  $m_1$  and  $m_2$  are component masses of the main binary;  $a_i$  is the semi-major axis of the main binary;  $m_3$  is the mass of the third component;  $e$  is the orbital eccentricity of the third component;  $q$  is the periastron distance of the third component orbit from the barycenter of the main binary; and  $\iota$  is the relative inclination of the third component orbit. This result can be used to investigate whether the component A is a binary system with an orbital period of 20 days (as was suggested by van Hoof, Bertiau, & Deurinck 1963).

In other words, we consider a hierarchical system with an inner binary A–C and an external component B. Assuming  $m_1 = 13 M_\odot$  (see Sect. 3.4), the semi-major axis of a body at a  $T = 20$ –day orbit is  $\sqrt[3]{Gm_1T^2/(4\pi^2)} = 0.35$  AU. Such a triple system is stable if component B does not come closer than 1.65 AU to the center of the A–C pair. The observations show that components A and B get as close together as 0.8 AU (e.g., Miroschnichenko et al. 2001; Che et al. 2012). The ultimate fate of such a system is a breakdown at already the second revolution. We therefore concur with Miroschnichenko et al. (2001) that the 20 day period is spurious.

Next we modeled the evolution of a stable triple system with a component C that is external to the eccentric A–B binary by numerically solving a system of motion equations in Cartesian coordinates. We used the orbital parameters of the inner binary from Table 3. The masses were assumed to be 13 and 8.2  $M_\odot$  for the components A and B, respectively (see

Sect. 3.4). The goal was to constrain parameters of component C, which can be responsible for the observed difference of the radial velocity curves obtained in 2011 and in 2000 as well as for long-term period variations. The results show that there is no unique solution to this problem, although certain constraints on the external orbit can be placed. In particular, the semi-major axis of the component C orbit cannot be smaller than 67.5 AU and, therefore, its orbital period should be longer than 120 years.

As an example, we calculated radial velocity curves for a described above triple system with an external component C that has the following parameters: mass  $M_C = 1.5 M_\odot$ , semi-major axis  $a = 100$  AU, eccentricity  $e = 0.5$ , inclination of the orbit to the orbital plane of the inner binary  $i_C = 60^\circ$ , periastron longitude  $\omega_C = 30^\circ$ , and the mean anomaly  $E = 0^\circ$  for 2011 July 4. Two consecutive orbital cycles of this system demonstrate that the radial velocity curve can change similarly to the observed behavior for  $\delta$  Sco (Fig. 6a), while twenty of them show how orbital period can change over one orbit of the external component (Fig. 6b).

The mechanism responsible for the orbital variations of the inner binary is known as the above mentioned Lidov-Kozai resonance. It occurs in hierarchical triple systems, in which the external component orbit is tilted with respect to that of the inner binary. This situation leads to precession of the orbits around the direction of the total moment of impulse of the system. Additionally, if the inclination between the inner and the outer orbit exceeds  $\sqrt{\arccos(3/5)}$ , the precession is accompanied by the angular momentum exchange between the orbits. The latter manifests itself by cyclic variations of both orbit eccentricities. A detailed analysis of this effect is given by Valtonen & Karttunen (2006).

Since the evolution of a binary system due to tidal friction could lead to a secular decrease of the orbital eccentricity (e.g., Zahn 2008), it is likely that the large current eccentricity of the  $\delta$  Sco system implies an inclination of the component C orbit of  $\geq 40^\circ$ . This limits the set of orbital solutions capable of explaining the observed radial velocity variations.

Component C can be located as far as  $0''.3$  to  $0''.8$  from the center of mass of the inner binary, but it has not been detected yet. We can suggest several explanations for this result. First, the component C orbital period is very long (213 years for the orbital solution shown in Fig. 6). If component C is a normal star born in the same cluster, it should be nearly 8 mag fainter (for  $M = 1.5 M_\odot$ , Ekström et al. 2012) than component A. Such a faint star can probably be directly detected by interferometry, which has only been used to observe the system for the last  $\sim 40$  years. During this time period, component C might have been projectionally close to the inner binary. Also, the high brightness contrast might have hampered the detection.



## 5. Conclusions

The spectroscopic observational campaign of the 2011 periastron passage in the  $\delta$  Sco system was successful and resulted in a new measurement of the orbital period ( $10.8092 \pm 0.0005$  years or  $3948.0 \pm 1.8$  days). We also determined orbital elements using the radial velocity curve for the He II 4686 Å line which turned out to be very close to those found from the H $\alpha$  radial velocity data during the previous periastron passage in 2000. Using the new orbital solution and recent evolutionary models with rotation (Ekström et al. 2012), we derived new masses of the binary components corrected for gravity darkening of the primary (13 and 8.2  $M_{\odot}$ ). These estimates along with the refined angular semi-major axis of the binary orbit (Che et al. 2012) imply that  $\delta$  Sco is located at a distance of 137 pc from the Sun that is consistent with both alternative solutions for the HIPPARCOS parallax. The radial velocity and line profile variations observed in the H $\alpha$  line near the 2011 periastron were affected by the interaction of the secondary component and the CS disk around the primary component. Using these data, we estimated a disk radius of 150  $R_{\odot}$ . This result is consistent with previous interferometric measurements of the disk radius (e.g., Meilland et al. 2011) and indicates that the disk was most likely growing during the entire time between the last two periastron passages.

We have detected a signature of the secondary component, but not clearly revealed its properties. This result is consistent with an early B-type spectral type for this component. The radial velocity curve for the He II line slightly deviates from that derived in 2000 for the H $\alpha$  line. This result along with the high eccentricity of the system and the presence of a bow shock-like structure around it suggest that  $\delta$  Sco might have a third component, external to the interferometric binary, and be a runaway object, dynamically ejected from its parent cluster. If the third component is indeed present, then the orbital elements presented in Table 3 may change in the future. The system needs constant observational attention to verify this suggestion.

Finally, the campaign confirmed that amateur spectroscopy becomes an important factor in astronomy of emission-line stars. It is very important to continue observing  $\delta$  Sco spectroscopically, photometrically, and interferometrically to search for more clues about the nature of this unusual stellar system.

This work was supported in part by DGAPA/PAPIIT project IN 103912. A. M. acknowledges financial support from the University of North Carolina at Greensboro and from its Department of Physics and Astronomy. A. M., J. R., A. F., and T. G. thank the Instituto de Astrofísica de Canarias and its staff for allocating observing time and for technical, logistical and financial support, as well as for their hospitality during the observing run at

the Teide Observatory. J. R. thanks Alex Abad, Emilio Cadavid and all the staff that they direct for the technical support in preparation and during the mission at the IAC80 telescope. A. C. C. acknowledges support from CNPq (grant 308985/2009–5) and Fapesp (grant 2010/19029–0). This research has made use of the SIMBAD database, operated at CDS, Strasbourg, France and the BeSS database, operated at LESIA, Observatoire de Meudon, France (accessible at <http://basebe.obspm.fr>).

## REFERENCES

- Allen, C., & Poveda, A. 1974, In “The stability of the solar system and of small stellar systems”, Dordrecht, D. Reidel Publishing Co., 239
- Beardsley, W. R. 1969, Publications of the Allegheny Observatory of the University of Pittsburgh, Vol. VIII, No. 7, 91
- Bjorkman, K. S., Miroshnichenko, A. S., McDavid, D. A., & Pogrosheva, T. M. 2002, *ApJ*, 573, 812
- Brown, A. G. A., & Verschueren, W. 1997, *A&A*, 319, 811
- Carciofi, A. C., Miroshnichenko, A. S., Kusakin, A. V., et al. 2006, *ApJ*, 652, 1617
- Che, X., Monnier, J. D., Tycner, C., et al. 2012, *ApJ*, 757, 29
- Côté, J., & van Kerkwijk, M. H. 1993, *A&A*, 274, 870
- de Zeeuw, P. T., Hoogerwerf, R., de Bruijne, J. H. J., Brown, A. G. A., & Blaauw, A. 1999, *AJ*, 117, 354
- Donati, J.-S., Semel, M., Carter, B. D., Rees, D. E., & Collier Cameron, A. 1997, *MNRAS*, 291, 658
- Dworetzky, M. M. 1983, *MNRAS*, 203, 917
- Eggleton, P. P. 1983, *ApJ*, 268, 368
- Ekström, S., Georgy, C., Eggenberger, P., et al. 2012, *A&A*, 537, A146
- ESA 1997, The Hipparcos Catalogue, ESA SP-1200
- Fabregat, J., Reig, P., & Otero, S. 2000, *IAU Circ.*, No. 7461
- Fahed, R., Moffat, A. F. J., Zorec, J., et al. 2011, *MNRAS*, 418, 2

- Frost, E. B., Barrett, S. B., & Struve, O. 1926, *ApJ*, 64, 1
- Glebocki, R., & Gnacinski, P. 2005, *VizieR On-line Data Catalog: III/244*
- Gvaramadze, V. V., Pflamm-Altenburg, J., & Kroupa, P. 2011, *A&A*, 525, A17
- Gvaramadze, V. V., & Menten, K.M. 2012, *A&A*, 541, A7
- Gvaramadze, V. V., Weidner, C., Kroupa, P., & Pflamm-Altenburg, J. 2012, *MNRAS*, 424, 3037
- Haubois, X., Carciofi, A.C., Rivinius, T., Okazaki, A.T., & Bjorkman, J.E. 2012, *ApJ*, 756, 156
- Hartkopf, W. I., Mason, B. D., McAlister, H. A., et al. 1996, *AJ*, 111, 936
- Hills, J.S. 1975, *AJ*, 80, 809
- Hoffer, J.B. 1983, *AJ*, 88, 1420
- Hoffleit, D., & Jaschek, C. 1991, *The Bright star catalogue*, New Haven, Conn.: Yale University Observatory
- Kaufer, A., Stahl, O., Tubbesing, S., et al. 2000, *SPIE*, 4008, 459
- Koubský, P. 2005, *Ap&SS*, 296, 165
- Koubský, P., Hummell, C.A., Harmanec, P., et al. 2010, *A&A*, 517, A24
- Kozai, Y. 1962, *AJ*, 67, 591
- Kroupa, P. 1998, *MNRAS*, 298, 231
- Leonard, P. J. T., & Duncan, M. J. 1990, *AJ*, 99, 608
- Levato, H., Malaroda, S., Morell, N., & Soliveila, G. 1987, *ApJS*, 64, 487
- Lidov, M.L. 1962, *Planetary and Space Science*, 9, 719
- Meilland, A., Delaa, O., Stee, Ph., et al. 2011, *A&A*, 532, A80
- Melnik, A.M., & Dambis, A.K. 2009, *MNRAS*, 400, 518
- Millan-Gabet, R., Monnier, J. D., Touhami, Y., et al. 2010, *ApJ*, 723, 544
- Miroshnichenko, A. S., Fabregat, J., Bjorkman, K. S., et al. 2001, *A&A*, 377, 485

- Miroshnichenko, A. S., Bjorkman, K. S., Morrison, N. D., et al. 2003, *A&A*, 408, 305
- Miroshnichenko, A. S. 2009, *Be Star Newsletter*, No. 39
- Moultaka, J., Ilovaisky, S. A., Prugniel, P., Soubiran, C. 2004, *PASP*, 116, 693
- Nemravová, J., Harmanec, P., Koubský, P., et al. 2012, *A&A*, 537, A59
- Pecaut, M. J., Mamajek, E. E., Bubar, E. J. 2012, *ApJ*, 746, 154
- Peri, C. S., Benaglia, P., Brookes, D. P., Stevens, I. R., Isequilla, N. L. 2012, *A&A*, 538, A108
- Reid, M. J., Menten, K. M., Zheng, X. W., Brunthaler, A., Xu, Y. 2009, *ApJ*, 705, 1548
- Reig, P., Fabregat, J., & Coe, M. 1997, *A&A*, 322, 193
- Rivinius, T., Štefl, S., Baade, D., Carciofi, A. C., Otero, S., Miroshnichenko, A. S., & Manset, N. 2012, in *Circumstellar Dynamics at High Resolution*, eds. A. Carciofi and Th. Rivinius, *ASP Conf. Ser.*, 464, 235
- Scargle, J.D. 1982, *ApJ*, 263, 835
- Schönrich, R., Binney, J., & Dehnen, W. 2010, *MNRAS*, 403, 1829
- Štefl, S., LeBouquin, J.-B., Rivinius, T., et al. 2012, in *Circumstellar Dynamics at High Resolution*, eds. A. Carciofi and Th. Rivinius, *ASP Conf. Ser.*, 464, 197
- Thackeray, A.D. 1966, *MmRAS*, 70, 33
- Tango, W. J., Davis, J., Jacob, A. P., et al. 2009, *MNRAS*, 396, 842
- Townsend, R. H. D., Owocki, S. P., & Howarth, I. D. 2004, *MNRAS*, 350, 189
- Tycner, C., Ames, A., Zavala, R. T., et al. 2011, *ApJ*, 729, L5
- Valtonen, M., & Karttunen, H. 2006, *The Three-Body Problem*, Cambridge UK, Cambridge University Press
- Valtonen, M., Mylläri, A., Orlov, V., Rubinov, A. 2008, in *Dynamical Evolution of Dense Stellar Systems*, *Proc. IAU Symp.* 246, 209
- van Buren, D., Noriega-Crespo, A., & Dgani, R. 1995, *AJ*, 110, 2914
- van Hoof, A., Bertiau, F.C., & Deurinck, R. 1963, *ApJ*, 137, 824

van Leeuwen, F. 2007, *A&A*, 474, 653

Werner, M. W., Roellig, T. L., Low, F. J., et al. 2004, *ApJS*, 154, 1

Wright, E. L., Eisenhardt, P. R. M., Mainzer, A. K., et al. 2010, *AJ*, 140, 1868

Zahn, J.-P. 2008, *EAS Publications Series*, 29, 67

Table 1: Radial velocities for the H $\alpha$  line

Date MM/DD/YYYY	JD2450000+ days	RV km s <sup>-1</sup>	Error km s <sup>-1</sup>	Source
05/28/2010	5344.835	-2.6	0.5	1
05/30/2010	5346.835	-1.7	0.6	1
06/03/2010	5350.779	-2.0	0.5	1
06/04/2010	5351.802	-2.5	0.2	1
06/19/2010	5366.766	-3.5	0.1	1
06/22/2010	5369.747	-2.7	0.3	1
06/25/2010	5372.901	-4.0	0.1	1
07/22/2010	5399.741	-0.5	0.3	1
07/25/2010	5402.743	-1.3	0.2	1
07/27/2010	5404.763	-0.6	0.1	1
07/31/2010	5408.742	-1.2	0.2	1
08/05/2010	5413.842	-2.3	0.9	1
10/05/2010	5474.929	-3.5	0.6	6
10/10/2010	5479.927	-3.8	1.5	6
10/21/2010	5490.913	-6.0	0.3	6
01/10/2011	5571.762	-15.1	3.4	4
01/16/2011	5577.729	-14.5	3.0	4
01/20/2011	5581.745	-13.4	3.1	4
01/23/2011	5584.749	-14.1	3.0	4
01/23/2011	5585.363	-14.9	2.2	2
01/28/2011	5589.704	-15.7	1.6	8
01/30/2011	5591.707	-12.8	1.8	8
02/09/2011	5601.725	-11.2	3.0	4
03/07/2011	5628.349	-6.7	2.3	2
03/09/2011	5629.641	-14.1	2.7	9
03/10/2011	5630.658	-14.1	3.0	9
03/13/2011	5634.399	-7.3	2.2	2
03/16/2011	5637.392	-7.4	2.8	2
03/29/2011	5649.566	-17.7	1.2	8
04/05/2011	5656.605	-17.5	2.4	9
04/06/2011	5657.558	-19.1	2.6	9
04/09/2011	5660.542	-13.9	4.7	5
04/15/2011	5667.488	-11.0	3.6	5

Table 1. continued

Date MM/DD/YYYY	JD2450000+ days	RV km s <sup>-1</sup>	Error	Source
04/16/2011	5668.391	-6.4	1.1	2
04/25/2011	5677.378	-7.0	1.1	2
04/27/2011	5678.600	-13.2	3.9	5
04/30/2011	5681.561	-16.5	5.6	5
05/03/2011	5685.514	-11.1	4.9	4
05/11/2011	5692.535	-11.7	5.2	4
05/20/2011	5702.463	-10.9	1.0	5
05/22/2011	5704.443	-16.8	5.1	4
05/27/2011	5709.507	-13.0	0.9	5
05/28/2011	5709.573	-12.1	0.4	4
05/29/2011	5710.400	-11.9	3.3	4
06/01/2011	5713.960	-14.5	0.8	6
06/01/2011	5714.371	-23.5	2.4	8
06/02/2011	5715.381	-15.8	1.6	8
06/08/2011	5720.529	-18.3	2.0	1
06/08/2011	5721.026	-18.4	2.1	1
06/08/2011	5721.395	-24.7	2.0	8
06/09/2011	5722.407	-19.7	1.8	1
06/11/2011	5723.797	-19.1	0.3	6
06/11/2011	5724.445	-22.8	3.9	7
06/12/2011	5725.318	-21.6	1.9	1
06/14/2011	5727.387	-32.3	2.4	8
06/14/2011	5727.436	-29.6	4.8	4
06/14/2011	5727.446	-26.7	2.6	5
06/15/2011	5728.459	-33.7	7.3	4
06/16/2011	5729.269	-26.9	1.8	1
06/16/2011	5729.380	-43.0	3.2	8
06/18/2011	5731.406	-31.2	1.3	5
06/21/2011	5734.412	-42.5	3.6	8
06/22/2011	5735.087	-34.9	1.8	2
06/22/2011	5735.380	-42.2	3.9	8
06/24/2011	5737.394	-45.4	4.5	8
06/26/2011	5738.984	-41.9	1.2	2

Table 1. continued

Date MM/DD/YYYY	JD2450000+ days	RV km s <sup>-1</sup>	Error	Source
06/26/2011	5739.387	-49.4	0.6	8
06/27/2011	5740.374	-52.2	0.3	8
06/28/2011	5741.503	-49.4	1.0	3
06/29/2011	5741.939	-51.0	0.4	6
06/29/2011	5742.396	-49.5	0.8	3
07/01/2011	5743.905	-50.6	1.5	6
07/01/2011	5744.301	-49.4	0.7	1
07/02/2011	5744.555	-49.2	0.3	3
07/02/2011	5745.241	-47.9	0.9	1
07/03/2011	5745.502	-48.1	0.3	4
07/03/2011	5745.543	-47.4	0.5	3
07/03/2011	5746.119	-47.4	0.6	6
07/03/2011	5746.241	-48.4	1.4	1
07/04/2011	5746.521	-47.0	1.4	3
07/04/2011	5746.938	-50.0	1.5	6
07/04/2011	5747.377	-49.4	2.3	4
07/04/2011	5747.428	-49.2	1.9	1
07/05/2011	5747.549	-48.8	1.6	3
07/05/2011	5748.383	-52.6	1.1	8
07/05/2011	5748.407	-47.9	2.1	1
07/06/2011	5748.548	-48.6	1.7	3
07/06/2011	5749.122	-49.2	2.0	2
07/07/2011	5749.549	-47.6	1.5	3
07/07/2011	5750.409	-44.5	0.2	8
07/07/2011	5750.432	-49.0	0.8	1
07/08/2011	5750.546	-46.7	1.8	3
07/08/2011	5751.372	-44.7	1.6	8
07/09/2011	5751.880	-41.5	1.0	6
07/09/2011	5752.259	-39.6	0.5	1
07/10/2011	5753.090	-42.0	1.0	2
07/11/2011	5754.085	-44.8	1.5	2
07/11/2011	5754.366	-50.1	3.4	8
07/13/2011	5755.976	-44.1	1.3	2



Table 1. continued

Date MM/DD/YYYY	JD2450000+ days	RV km s <sup>-1</sup>	Error	Source
07/13/2011	5756.189	-43.9	1.1	2
07/13/2011	5756.281	-44.2	1.3	1
07/14/2011	5756.897	-42.1	1.0	6
07/14/2011	5757.211	-43.6	0.7	2
07/14/2011	5757.388	-43.6	1.0	1
07/15/2011	5757.882	-46.5	2.4	6
07/15/2011	5758.371	-45.9	1.2	8
07/17/2011	5759.961	-38.3	1.0	2
07/17/2011	5760.245	-37.9	1.2	2
07/17/2011	5760.398	-38.4	1.8	4
07/20/2011	5762.932	-34.8	1.4	6
07/20/2011	5763.372	-32.1	1.4	8
07/20/2011	5763.383	-35.4	2.0	4
07/21/2011	5764.440	-31.2	3.8	4
07/22/2011	5764.952	-32.2	0.7	2
07/22/2011	5765.450	-32.3	5.3	4
07/23/2011	5765.963	-31.7	1.2	2
07/23/2011	5766.362	-32.2	1.0	4
07/23/2011	5766.393	-29.7	0.8	8
07/24/2011	5766.974	-30.6	1.6	2
07/25/2011	5768.086	-29.8	1.1	2
07/26/2011	5769.085	-29.6	1.3	2
07/29/2011	5772.346	-27.3	0.7	5
07/30/2011	5773.360	-26.0	1.2	5
08/01/2011	5775.347	-24.2	0.7	5
08/02/2011	5776.345	-23.2	0.7	5
08/03/2011	5777.344	-22.2	1.4	5
08/04/2011	5778.356	-22.0	0.9	5
08/05/2011	5779.348	-20.8	1.2	5
08/11/2011	5784.968	-15.4	1.5	6
08/12/2011	5786.012	-16.1	1.8	6
08/14/2011	5788.024	-14.8	1.0	6

Table 1. continued

Date MM/DD/YYYY	JD2450000+ days	RV km s <sup>-1</sup>	Error	Source
08/16/2011	5790.228	-14.5	0.5	1
08/19/2011	5793.331	-10.5	3.4	5
08/27/2011	5800.985	-9.4	2.2	2
08/28/2011	5801.972	-9.4	2.0	2
08/29/2011	5803.065	-9.0	2.3	2
08/30/2011	5804.044	-10.7	2.5	2
08/31/2011	5805.001	-11.2	2.4	2
09/01/2011	5806.053	-12.9	3.5	2
09/02/2011	5807.025	-11.9	2.9	2
09/04/2011	5808.998	-11.0	1.9	2
09/05/2011	5809.963	-10.0	2.7	6
09/05/2011	5809.995	-12.0	1.8	2
09/05/2011	5810.023	-8.7	2.9	6
09/06/2011	5810.982	-11.4	2.6	2
09/07/2011	5811.990	-10.9	2.4	2
10/02/2011	5836.916	-10.1	1.2	6
10/12/2011	5846.913	-11.7	0.2	6

Column information: (1) – Observing date, (2) – Julian date, (3) – measured heliocentric radial velocity, (4) – r.m.s. error of the mirrored fit to the line profile, (5) – source of the spectrum: 1 – ESPaDOnS (CFHT), 2 – FEROS at the 1.52m ESO telescope, 3 – IAC80 telescope of the Teide Observatory, 4 – C. Buil, 5 – T. Garrel, 6 – B. Heathcote, 7 – J. Ribeiro, 8 – E. Pollmann, 9 – O. Thizy.

Table 2: Radial velocities for the He II 4686 Å line

Date MM/DD/YYYY	JD2450000+ days	RV km s <sup>-1</sup>	Error	Source
5/28/2010	5344.835	-10.7	0.0035	1
5/30/2010	5346.835	-12.8	0.0014	1
6/3/2010	5350.779	-7.7	0.0028	1
6/4/2010	5351.802	-8.7	0.0017	1
6/19/2010	5366.766	-10.7	0.0018	1
6/22/2010	5369.747	-9.7	0.0019	1
6/25/2010	5372.901	-13.8	0.0020	1
7/22/2010	5399.741	-9.7	0.0019	1
7/25/2010	5402.743	-9.7	0.0020	1
7/27/2010	5404.763	-10.7	0.0026	1
7/31/2010	5408.742	-9.7	0.0025	1
8/5/2010	5413.842	-11.7	0.0030	1
1/10/2011	5571.762	-20.5	0.0021	4
1/16/2011	5577.729	-14.8	0.0039	4
1/20/2011	5581.745	-14.2	0.0030	4
1/23/2011	5584.749	-11.7	0.0034	4
1/23/2011	5585.363	-11.8	0.0027	2
2/9/2011	5601.725	-13.0	0.0027	4
3/6/2011	5626.717	-19.4	0.0025	4
3/7/2011	5628.349	-21.9	0.0033	2
3/13/2011	5634.399	-14.0	0.0054	2
3/16/2011	5637.392	-12.1	0.0038	2
3/25/2011	5645.632	-18.0	0.0040	4
4/16/2011	5667.567	-14.0	0.0029	4
4/16/2011	5667.603	-8.2	0.0026	7
4/16/2011	5668.391	-17.0	0.0038	2
4/25/2011	5677.378	-6.9	0.0038	2
4/28/2011	5679.559	-24.6	0.0030	4
5/3/2011	5685.514	-13.8	0.0025	4
5/11/2011	5692.535	-15.5	0.0031	4
5/17/2011	5699.491	-17.1	0.0038	5

Table 2. continued

Date MM/DD/YYYY	JD2450000+ days	RV km s <sup>-1</sup>	Error	Source
5/20/2011	5702.431	-23.2	0.0037	5
5/21/2011	5703.053	-17.3	0.0019	6
5/22/2011	5704.443	-21.5	0.0039	4
5/24/2011	5706.427	-20.9	0.0031	5
5/27/2011	5709.507	-18.8	0.0038	5
5/28/2011	5709.573	-22.8	0.0025	4
5/28/2011	5710.400	-24.2	0.0031	4
6/7/2011	5721.026	-29.8	0.0028	1
6/10/2011	5722.405	-25.5	0.0043	1
6/12/2011	5724.565	-41.1	0.0039	7
6/14/2011	5727.436	-28.1	0.0027	4
6/14/2011	5727.446	-30.7	0.0039	5
6/15/2011	5728.459	-29.7	0.0038	4
6/17/2011	5729.268	-29.6	0.0023	1
6/18/2011	5731.396	-43.9	0.0031	4
6/18/2011	5731.406	-34.7	0.0031	5
6/22/2011	5735.087	-39.7	0.0060	2
6/25/2011	5738.984	-48.2	0.0044	2
6/26/2011	5739.359	-42.9	0.0033	4
6/29/2011	5742.396	-57.5	0.0035	3
6/29/2011	5742.921	-55.8	0.0063	6
7/1/2011	5743.551	-53.0	0.0027	3
7/1/2011	5743.880	-49.9	0.0059	6
7/1/2011	5744.374	-51.5	0.0023	4
7/2/2011	5745.415	-57.2	0.0027	3
7/2/2011	5745.480	-53.6	0.0029	4
7/3/2011	5746.105	-56.6	0.0069	6
7/4/2011	5746.938	-54.6	0.0047	6
7/5/2011	5747.362	-52.6	0.0040	4
7/6/2011	5748.419	-44.2	0.0260	3
7/6/2011	5748.453	-51.5	0.0032	4
7/6/2011	5749.122	-47.2	0.0040	2

Table 2. continued

Date MM/DD/YYYY	JD2450000+ days	RV km s <sup>-1</sup>	Error	Source
7/9/2011	5751.354	-38.2	0.0027	4
7/9/2011	5751.880	-37.9	0.0094	6
7/10/2011	5752.358	-44.2	0.0029	4
7/10/2011	5753.090	-46.9	0.0042	2
7/11/2011	5753.360	-49.6	0.0031	4
7/11/2011	5753.397	-35.9	0.0035	4
7/11/2011	5754.085	-38.5	0.0037	2
7/12/2011	5754.352	-48.0	0.0026	4
7/12/2011	5755.976	-39.4	0.0043	2
7/13/2011	5756.189	-38.6	0.0047	2
7/14/2011	5756.880	-31.3	0.0029	5
7/14/2011	5756.897	-29.0	0.0064	6
7/14/2011	5757.211	-32.9	0.0058	2
7/15/2011	5757.882	-29.4	0.0057	6
7/17/2011	5759.961	-34.1	0.0048	2
7/17/2011	5760.245	-34.3	0.0036	2
7/18/2011	5760.373	-36.9	0.0021	4
7/20/2011	5762.932	-26.1	0.0041	6
7/21/2011	5763.363	-28.0	0.0026	4
7/22/2011	5764.426	-30.3	0.0035	4
7/22/2011	5764.952	-32.6	0.0035	2
7/22/2011	5764.961	-31.2	0.0050	6
7/23/2011	5765.963	-32.6	0.0037	2
7/24/2011	5766.974	-28.6	0.0050	2
7/25/2011	5768.086	-31.6	0.0039	2
7/26/2011	5768.947	-27.4	0.0053	6
7/26/2011	5769.085	-28.0	0.0038	2
7/27/2011	5770.071	-25.8	0.0057	6
7/28/2011	5770.969	-23.6	0.0052	6
7/29/2011	5772.343	-25.9	0.0038	5

Table 2. continued

Date MM/DD/YYYY	JD2450000+ days	RV km s <sup>-1</sup>	Error	Source
7/31/2011	5774.007	-23.0	0.0061	6
8/3/2011	5777.056	-28.2	0.0730	6
8/3/2011	5777.334	-25.1	0.0041	5
8/5/2011	5779.335	-23.3	0.0042	5
8/11/2011	5784.953	-24.2	0.0056	6
8/12/2011	5785.994	-15.5	0.0044	6
8/14/2011	5788.023	-20.7	0.0080	6
8/27/2011	5800.985	-24.4	0.0020	2
8/28/2011	5801.972	-19.8	0.0037	2
8/29/2011	5803.065	-16.1	0.0043	2
8/30/2011	5804.044	-17.6	0.0038	2
8/31/2011	5805.001	-18.3	0.0022	2
9/1/2011	5806.053	-13.6	0.0034	2
9/2/2011	5807.025	-15.1	0.0043	2
9/4/2011	5808.998	-17.4	0.0025	2
9/5/2011	5809.963	-17.9	0.0054	6
9/5/2011	5809.995	-13.4	0.0025	2
9/6/2011	5810.982	-12.6	0.0048	2
9/7/2011	5811.990	-18.1	0.0037	2
9/8/2011	5812.983	-19.6	0.0051	6
10/2/2011	5836.916	-4.6	0.0049	6
10/12/2011	5846.913	-5.1	0.0071	6

Column information: (1) – Observing date, (2) – Julian date, (3) – measured heliocentric radial velocity, (4) – r.m.s. error of the Gaussian fit to the line profile, (5) – source of the spectrum: 1 – ESPaDOnS (CFHT), 2 – FEROS at the 1.52m ESO telescope, 3 – IAC80 telescope of the Teide Observatory, 4 – C. Buil, 5 – T. Garrel, 6 – B. Heathcote, and 7 – J. Ribeiro.

Table 3: Orbital solutions for  $\delta$  Sco

$T_0$ days	$K_1$ $\text{km s}^{-1}$	$e$	$\gamma$ $\text{km s}^{-1}$	$\omega$ degrees	Reduced $\chi^2$	N
$2451797.9 \pm 1.0$	$23.9 \pm 1.1$	$0.937 \pm 0.002$	$-5.8 \pm 1.2$	$-1.3 \pm 3.5$	0.82	30
$2455745.9 \pm 0.9$	$23.4 \pm 0.5$	$0.936 \pm 0.004$	$-7.7 \pm 0.8$	$-2.6 \pm 3.0$	0.74	25
$2455745.9 \pm 1.0$	$23.9 \pm 0.8$	$0.936 \pm 0.003$	$-6.6 \pm 1.0$	$-2.3 \pm 3.8$	0.92	55

$T_0$  is the periastron passage epoch,  $K_1$  is the semi-amplitude of the radial velocity curve,  $e$  is the orbit eccentricity,  $\gamma$  is the systemic radial velocity,  $\omega$  is the periastron longitude, N is the number of data points in a set. The first line lists the best fit parameters for the periastron 2000 H $\alpha$  line radial velocity data set, the second line shows the same for the 2011 He II 4686 Å line, and the third line shows the same for the combined data set.

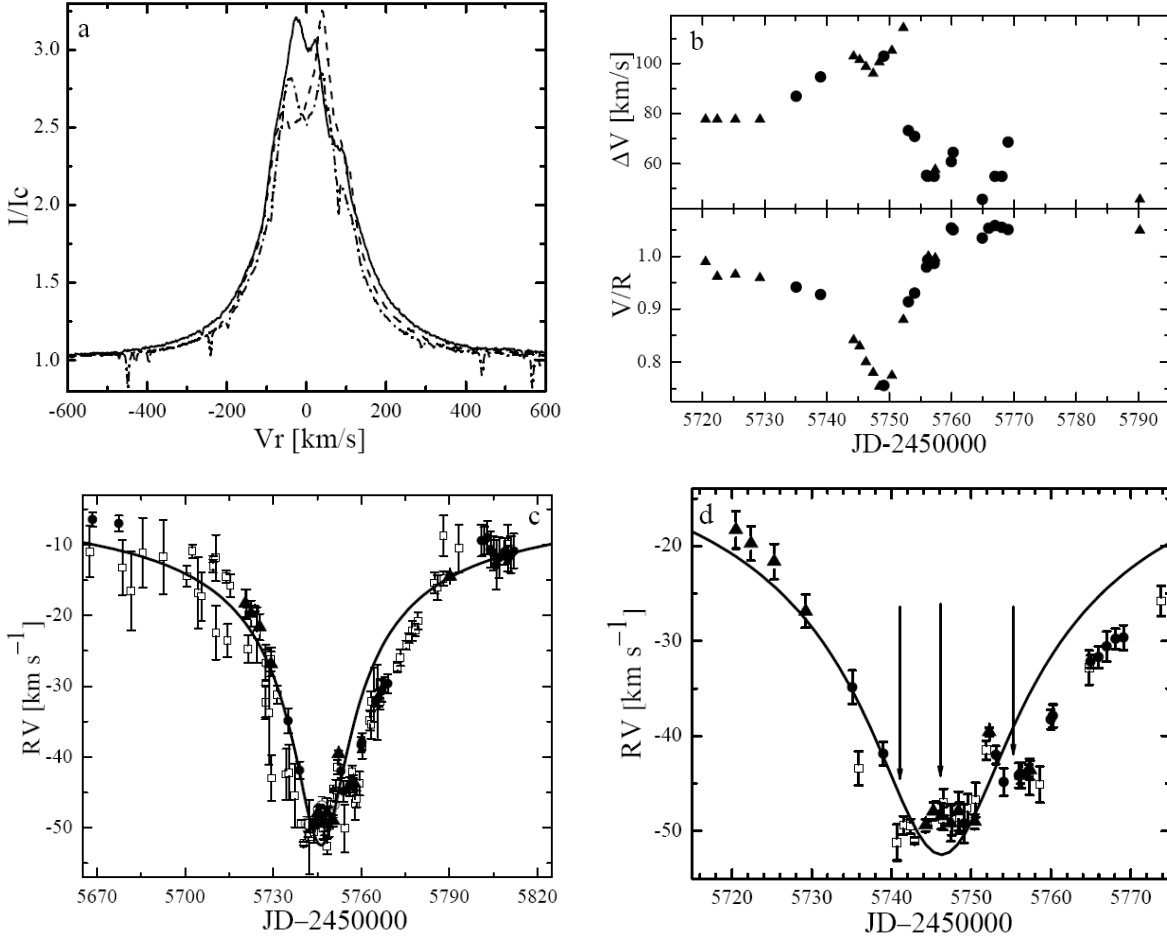


Fig. 1.— The profile and radial velocity variations of the H $\alpha$  line in the spectrum of  $\delta$  Sco around the periastron time. **Panel a:** the line profile variations. CFHT spectra on three dates are shown: 2011 June 8 (solid line), 2011 July 4 (dashed line), and 2011 August 16 (dash-dotted line). The intensity is normalized to the nearby continuum, the radial velocity is heliocentric and shifted to the periastron time. No correction for telluric lines was done. **Panel b:** the line peak ratio and the peak separation. Symbols: filled circles—CFHT/ESPaDOnS data and filled triangles—ESO/FEROS data. **Panel c:** all radial velocity data obtained in March–October 2011. The heliocentric radial velocities in  $\text{km s}^{-1}$  are plotted against time in Julian dates. The solid line represents the best fit radial velocity curve to the data obtained during the 2000 periastron shifted by  $+6 \text{ km s}^{-1}$  (Miroshnichenko et al. 2001). Symbols: professional data—the same as in panel b), open squares—all amateurs data. **Panel d:** the heliocentric radial velocities for a shorter period of time near the periastron. Symbols are the same as in panel c), but the amateurs data are averaged within 2–3 day periods. The arrows mark three minima (see text). The central minimum roughly coincides with the periastron time.



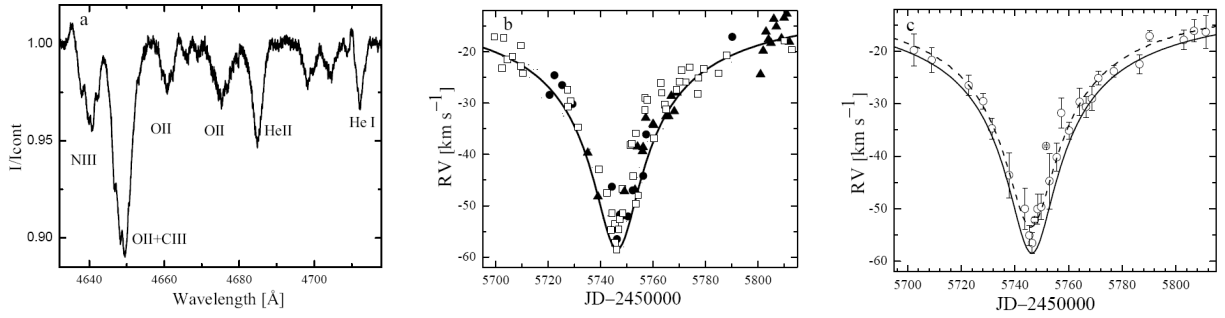


Fig. 2.— **Panel a:** Part of the 2011 July 4 CFHT spectrum near the He II 4686 Å line. Intensities are normalized to the underlying continuum, and heliocentric wavelengths are given in Å. **Panel b:** Radial velocity data for the He II 4686 Å line in the spectrum of  $\delta$  Sco. The radial velocities and time are given in the same units as in Fig. 1. The solid line represents the best fit heliocentric radial velocity curve to the data obtained during the 2000 periastron from Miroschnichenko et al. (2001), no shift is applied. **Panel c:** The same set of radial velocities for the He II 4686 Å line, but averaged over 2–3 day periods to decrease the individual data scatter. The professional and amateur data are mixed together on this plot. The solid line is the same as in the Panel b). The dashed line is the best fit for the averaged data from Table 3.

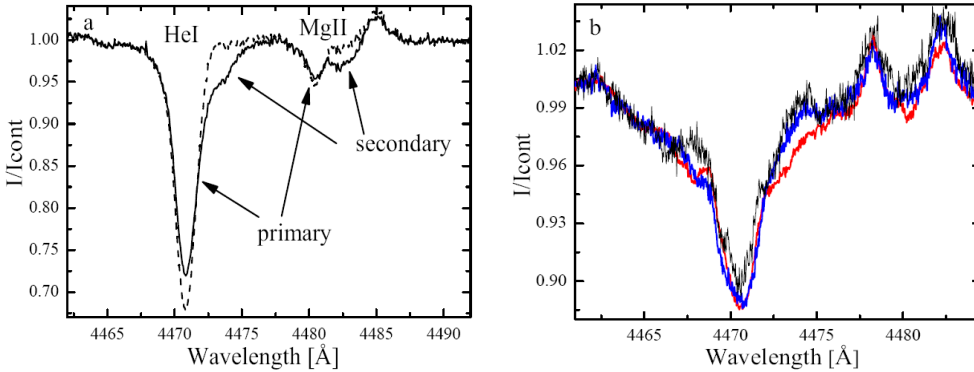


Fig. 3.— Possible effects of the secondary component on the spectrum of  $\delta$  Sco at periastron. Panel a) Solid line shows a sum of two spectra of BS 1880, a B0.5 V star (shown by a dashed line), and BS 801, a B3 V star, scaled with a brightness difference of  $\Delta B = 1.78$  mag. The components’ radial velocity difference is  $120 \text{ km s}^{-1}$ . Panel b) shows the CFHT spectra taken before (blus line, 2011 June 8), at (red line, 2011 July 4), and after the periastron (black line, 2011 August 16). The Mg II 4482 Å line has a double-peak emission profile. The wavelengths are shifted to the periastron epoch. Intensities and wavelengths are in the same units as in Fig. 2b.

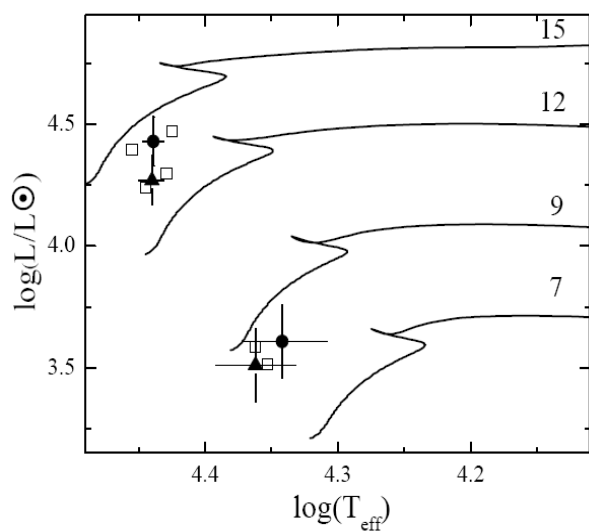


Fig. 4.— Part of a Hertzsprung–Russell diagram showing evolutionary tracks with rotation from Ekström et al. (2012). Initial masses in solar units are indicated by the numbers near corresponding tracks. No gravity darkening positions of the  $\delta$  Sco A and B components are shown by filled circles, while those with this effect accounted are shown by filled triangles. Open squares near component A positions indicate theoretical values for ages of 8 and 10 Myrs. Open squares near component B positions indicate theoretical values with an age of 10 Myrs for initial masses of  $8.6 M_{\odot}$  (upper square) and  $8.2 M_{\odot}$  (lower square).

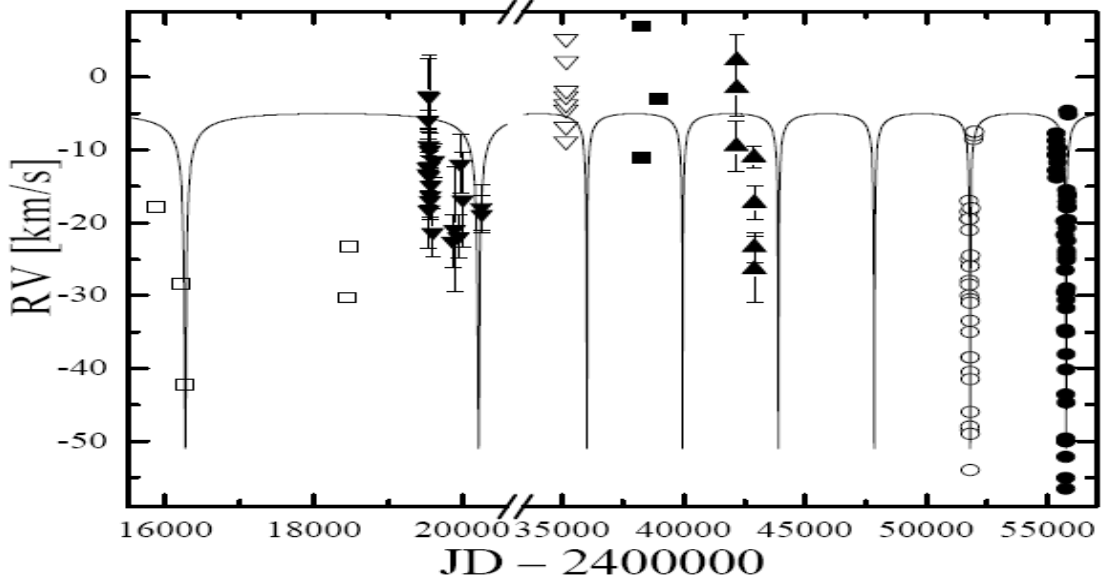


Fig. 5.— Radial velocities of  $\delta$  Sco measured since the early 20–th century. Symbols: open squares are data from Frost et al. (1926), filled downward triangles – Beardsley (1969), open downward triangles – van Hoof, Bertiau, & Deurinck (1963), filled squares – Thackeray (1966), filled upward triangles – Levato et al. (1987), open circles – Miroschnichenko et al. (2001), and filled circles – this work. The solid line represents the orbital solution for the 2011 periastron shown in Table 3 (see Sect. 3.1).

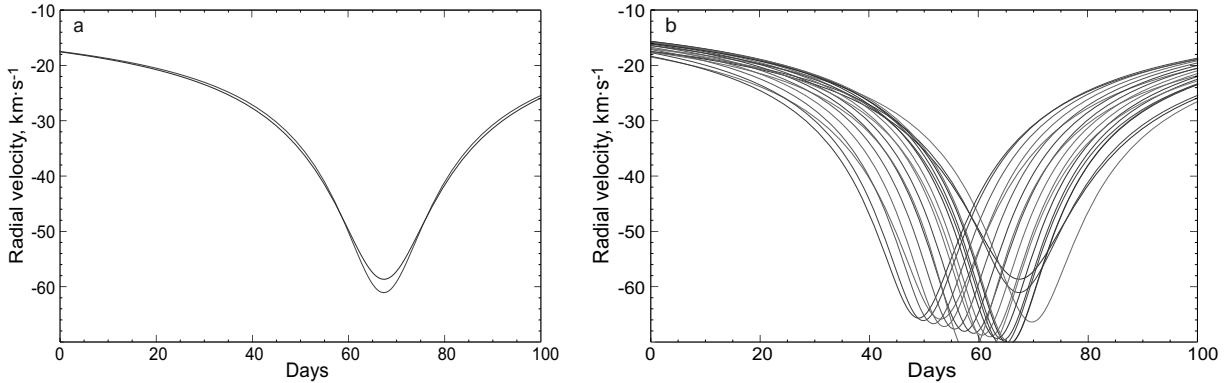


Fig. 6.— Panel a) shows radial velocity curves for two consecutive orbital cycles of a triple system that consists from an inner binary and an outer third component with the orbital parameters described in Sect. 4.3. Panel b) shows radial velocity curves for twenty consecutive orbital cycles of the inner binary from the same triple system that occur during one orbital period of the outer component. Time scale has an arbitrary zero-point.